Dye-Sensitized MoS_2 Photodetector with Enhanced Spectral Photoresponse

Seong Hun Yu,[†,⊗] Youngbin Lee,[‡,⊗] Sung Kyu Jang,[‡,⊗] Jinyeong Kang,[#] Jiwon Jeon,[▽] Changgu Lee,[‡,§] Jun Young Lee,[†] Hyungjun Kim,[▽] Euyheon Hwang,[‡,⊥] Sungjoo Lee,[‡,∥,*] and Jeong Ho Cho[†,‡,*]

[†]School of Chemical Engineering, [‡]SKKU Advanced Institute of Nanotechnology (SAINT), [§]School of Mechanical Engineering, [⊥]Department of Physics, and [∥]School of Electrical and Computer Engineering, Sungkyunkwan University, Suwon 440-746, Republic of Korea, [#]System LSI Etch Technology Team, Samsung Electronics, Giheung 446-711, Republic of Korea, and [▽]Graduate School of Energy Environment Water Sustainability (EEWS), Korea Advanced Institute of Science and Technology (KAIST), Daejeon 305-701, Republic of Korea. [⊗]These authors contributed equally to this work.

ABSTRACT We fabricated dye-sensitized MoS_2 photodetectors that utilized a single-layer MoS_2 treated with rhodamine 6G (R6G) organic dye molecules (with an optical band gap of 2.38 eV or 521 nm). The proposed photodetector showed an enhanced performance with a broad spectral photoresponse and a high photoresponsivity compared with the properties of the pristine MoS_2 photodetectors. The R6G dye molecules deposited onto the MoS_2 layer increased the photocurrent by an order of magnitude due to charge transfer of the photoexcited electrons from the R6G molecules to the MoS_2 layer. Importantly, the photodetection response extended to the infrared ($\lambda < 980$ nm, which corresponded to about half the energy band gap of MoS_2), thereby distinguishing the device performance from that of a pristine MoS_2 device, in which detection was only possible at wavelengths shorter than the band gap of MoS_2, *i.e.*, $\lambda < 681$ nm. The resulting device exhibited a maximum photoresponsivity of 1.17 AW^{-1}, a photodetectivity of 1.5×10^7 Jones, and a total effective quantum efficiency (EQE) of 280% at 520 nm. The device design described here presents a significant step toward high-performance 2D nanomaterial-based photodetector.

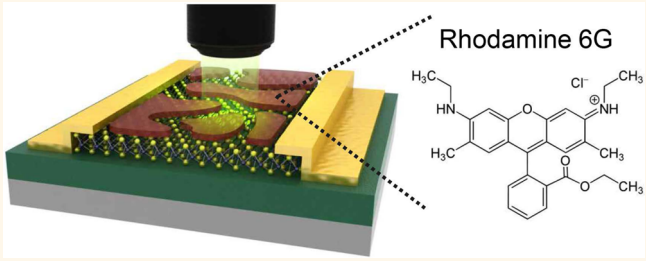

KEYWORDS: MoS_2 · photodetector · organic dye · broad spectral photoresponse · photoresponsivity

Photodetectors based on nanomaterials have attracted significant attention due to their large surface-to-volume ratio, good light sensitivity compared to the bulk materials, and long photocarrier lifetimes.[1−5] Compared to quantum dots (0D) and one-dimensional (1D) nanostructures, such as semiconducting nanowires and carbon nanotubes, two-dimensional (2D) nanomaterials are more compatible with established device designs and thin film microfabrication processes.[6−10] A variety of 2D nanomaterials have been fabricated to date. Graphene, in particular, yields an ultrahigh operation frequency with an ultrawide band operation that extends from the ultraviolet to the terahertz range as a result of the material's high carrier mobility, wide band absorption, and short carrier lifetime.[3,11−15] Despite the high-speed and broadband photodetection properties of graphene, practical optoelectronic applications of pristine graphene have been limited due to graphene's low photoresponsivity, photodetectivity, and very low external quantum efficiency, which originates from graphene's relatively low light absorption coefficient and the fast rate of photoinduced carrier recombination.[16−18] The disadvantages of graphene photodetectors may be overcome by replacing graphene with 2D semiconducting nanomaterials, such as molybdenum disulfide (MoS_2), gallium sulfide (GaS), and gallium selenide (GaSe), which feature a direct and finite band gap.[4,19−21] Two-dimensional semiconducting layered materials that are structurally similar to graphite may be built up from atomic planes that are held in contact by weak van der Waals forces. The atoms or molecules within each plane are covalently bonded, and atomically thin nanosheets may be isolated simply using mechanical exfoliation techniques. A few photodetectors based on single and multilayer 2D nanomaterials have been fabricated. These devices exhibited performances comparable to those obtained from commercial photodetectors.[2,5]

* Address correspondence to jhcho94@skku.edu, leesj@skku.edu.

Received for review May 18, 2014 and accepted July 25, 2014.

Published online July 25, 2014
10.1021/nn502715h

The performances of 2D photodetector devices can be further improved by introducing an active component into the top layer of a nanomaterial, such as graphene.[22−24] For example, quantum dots that exhibit strong wavelength-tunable light absorption characteristics significantly enhanced the light absorption and spectral selectivity of the photodetectors;[16,17,22,25] however, this approach relied on complex manipulations and the fabrication of quantum dots. The systematic control over the quantity of quantum dots adsorbed onto a target substrate remains challenging. The development of alternative low-cost simple methods is critical for practical applications of this strategy toward maximizing light absorption in photodetectors based on 2D nanomaterials.

This report introduces a simple method for enhancing the photoresponse of a pristine MoS_2 photodetector by utilizing organic dye molecules. Organic dye molecules have been widely applied in dye-sensitized solar cells (DSSCs) and are commonly used in the laser and medical fields due to their outstanding optical characteristics, including a wide optical absorption bandwidth and specific photoluminescence properties.[26−29] The commercially available Rhodamine 6G (R6G) organic dye may be simply drop-cast onto a MoS_2 surface to dramatically enhance the electrical response of the device to light due to photoinduced charge transfer from the R6G dye molecules to MoS_2. The photoresponse parameters, including the photoresponsivity, photodetectivity, and the total effective quantum efficiency (EQE) (*i.e.*, the external quantum efficiency in the presence of operational gain mechanisms) increased by a factor of 10 for the R6G-treated devices. Our optimized device displayed a photoresponsivity of 1.17 AW^{-1}, a photodetectivity of 1.5×10^7 Jones, an EQE of 280% at 520 nm, and a photoresponse over a broad spectral range of 980−405 nm. The low-cost facile deposition of solution-processable organic dye molecules represents a significant step toward optimizing photodetectors based on 2D nanomaterials.

RESULTS AND DISCUSSION

We began the fabrication of transistor-type MoS_2 photodetectors using the Scotch tape-based micromechanical cleavage method to exfoliate single-layer MoS_2. A heavily n-doped Si wafer was used as the gate electrode, and a thermally grown 300 nm thick SiO_2 layer with a specific capacitance of 11.6 nF/cm^2 provided the gate dielectric. After exfoliation of the MoS_2 nanosheets, single-layer MoS_2 flakes were positioned on the underlying SiO_2 gate dielectric layer. Electron beam lithography and metal evaporation were used to fabricate 5/50 nm thick Cr/Au source−drain electrodes. The R6G organic dye molecules were drop-cast onto the MoS_2 surfaces. The optical band gap of R6G was found to be 2.38 eV, based on the UV absorption spectrum, as shown in the inset of Figure 2b. This measurement was consistent with the calculated value of 2.23 eV (Supporting Information). Schematic diagrams of the photodetector based on the R6G-sensitized single-layer MoS_2 are presented in Figure 1a. Figure 1b exhibits optical microscopy top view images of the MoS_2 photodetector and the height profile of pristine single-layer MoS_2, measured using atomic force microscopy (AFM). The thickness of the MoS_2 flakes mounted on the SiO_2/Si substrates was determined to be 0.6 nm, indicating the presence of single-layer MoS_2, consistent with previous theoretical and experimental results.[19,30] Supporting Information Figure S1 shows the Raman spectra of pristine and R6G-sensitized MoS_2 flakes. The two characteristic Raman peaks of MoS_2 were apparent at 388.7 cm^{-1} (E^1_{2g} mode), corresponding to the planar vibration, and at 407.8 cm^{-1} (A_{1g} mode), corresponding to the vibration of the sulfides in the out-of-plane direction.[30,31] The difference between these frequencies, which provides an indicator of the number of layers present, was 19 cm^{-1} and corresponded to single-layer MoS_2, consistent with the AFM results. The calculated density of states (DOS) of the R6G/MoS_2 hybrid system shown in Figure 1c revealed that the Fermi level of the hybrid system was located approximately midway between the highest occupied molecular orbital (HOMO) of R6G and the bottom of the conduction band of MoS_2. The calculated band gap of R6G physisorbed onto MoS_2 was 1.937 eV (HOMO, −5.077 eV and LUMO, −3.140 eV), which was slightly lower than that of the isolated R6G (2.23 eV).[32,33]

Figure 2a shows the photoinduced transfer characteristics (I_D (drain current)−V_G (gate voltage)) of the photodetectors based on pristine and R6G-sensitized MoS_2 in the dark or under different illumination wavelengths at a constant optical power of 1 mW (drain voltage (V_D) = 0.1 V). Pristine MoS_2 transistors in the dark exhibited typical n-type behavior. The devices yielded an electron mobility as high as 1.2 cm^2/(V s) at room temperature with an on/off current ratio 10^4. The electron mobility was calculated using the following equation: $\mu_{lin} = (g_m/C_{ox}V_D) \times (L/W)$, where g_m is the transconductance, and C_{ox} and V_D are the dielectric capacitance and drain voltage, respectively. The pristine single layer MoS_2 photodetector did not respond significantly to light at wavelengths longer than the optical band gap of the single layer MoS_2 (1.82 eV, λ = 681 nm), but the photocurrent increased significantly as the wavelength decreased from 681 nm. Incident photons with energies exceeding 1.82 eV excited electrons from the valence band into the conduction band of MoS_2 (red line in Figure 1d). By contrast, the R6G-sensitized MoS_2 photodetector exhibited a much wider photoresponse of up to 980 nm. The photoresponse of the detector over the range 681 nm < λ < 980 nm, which is the forbidden optical absorption

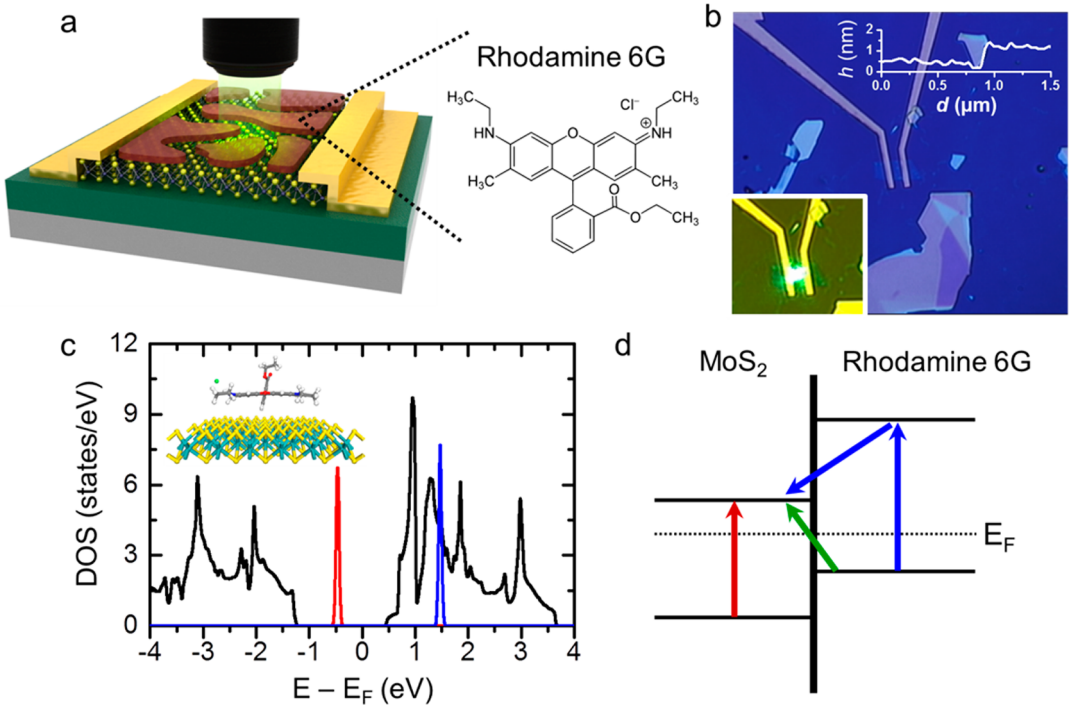

Figure 1. (a) Schematic diagram of the single-layer MoS_2 photodetectors treated with rhodamine 6G (R6G) organic dye molecules and chemical structure of the R6G dye. (b) Optical microscopy top-view images of the R6G-sensitized MoS_2 photodetectors. The inset shows the height profiles of the single-layer MoS_2. (c) MoS_2 monolayer DOS and the positions of the HOMO and LUMO in the physisorbed R6G. The black line represents the DOS of the MoS_2 monolayer. Red and blue lines represent the HOMO and LUMO of R6G, respectively, calculated using the B3PW91 methods, of the physisorbed R6G molecule, where the HOMO was located at −0.467 eV and the LUMO was located at 1.470 eV with respect to the Fermi level. The Fermi level of the composite system was selected to fall between the valence band maximum and the conduction band minimum, which were the HOMO of R6G and the conduction band minimum of MoS_2, respectively. (d) Schematic band diagram showing the R6G-sensitized MoS_2 photodetector under illumination.

region for pristine MoS_2 photodetectors, arose from the photoinduced electron transfer from the HOMO of R6G to the bottom of the conduction band of MoS_2 (green line in Figure 1d). Exposure of the R6G-sensitized MoS_2 photodetector to light with a photon energy exceeding the optical band gap of R6G (2.38 eV, λ = 521 nm), as shown in the UV absorption spectrum (the inset of Figure 2b), transferred electrons that had been excited from the HOMO to the LUMO of R6G to the conduction band of MoS_2, which dramatically increased the photocurrent in MoS_2 (blue line in Figure 1d). Consequently, the photoresponse behavior of MoS_2 was dramatically enhanced through the simple deposition of R6G organic dye molecules onto the MoS_2 surface. This difference was also observed in the output characteristics of both devices, as shown in Supporting Information Figure S4.

Figure 2b shows the photocurrent as a function of the wavelength obtained at a gate voltage of 0 V. The photocurrent obtained from the R6G-sensitized MoS_2 photodetector at 405 nm was higher than that obtained from the pristine MoS_2 photodetector by more than 1 order of magnitude. The enhanced photoresponse was observed at different gate voltages, as shown in Supporting Information Figure S5. The photoresponsivity (R) is a critical parameter for evaluating the performance of a photodetector. The photoresponsivity was calculated according to the equation $R = I_{ph}/P_{light}$, where I_{ph} is the generated photocurrent and P_{light} is the total incident optical power. Another important parameter for describing the detector performance is the photodetectivity (D^*), calculated according to $D^* = (RA^{1/2})/(2eI_d)^{1/2}$ if the shot noise from the DC is the major contributor to the noise. Here, A is the effective area of the detector, e is the absolute value of the electron charge (1.6×10^{-19} C), and I_d is the dark current.[34] The R and D^* values for various wavelengths for the pristine and R6G-sensitized MoS_2 photodetectors, collected at V_G = 0 V, are summarized in Figure 2c,d. The pristine MoS_2 device exhibited an R of 1.24×10^{-4} A W^{-1} and D^* of 2.4×10^4 Jones at 405 nm. By contrast, the R6G-sensitized MoS_2 yielded phototransistors with R and D^* values of 1.38×10^{-3} A W^{-1} and 3.5×10^5 Jones, respectively, more than 1 order of magnitude higher than the values obtained from the pristine MoS_2 device.

Figure 3a shows the photoinduced transfer curves of the pristine and R6G-sensitized MoS_2 photodetectors under 520 nm illumination over a range of optical powers. The plot of the photocurrent (I_{ph}) as a function of the incident optical power (P_{light}) is shown in Figure 3b and was obtained from the value of I_{ph} at a

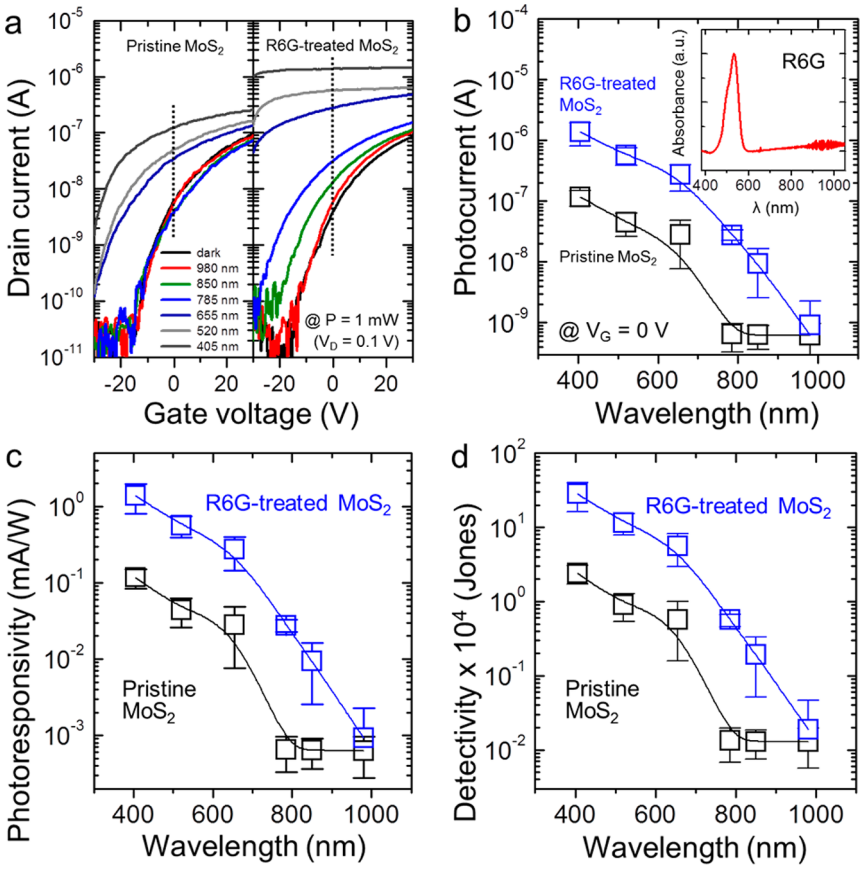

Figure 2. (a) Photoinduced transfer characteristics of the pristine and R6G-sensitized MoS_2 photodetectors under different illumination source wavelengths. (b) Photocurrent at $V_G = 0$ V, (c) photoresponsivity, and (d) photodetectivity as a function of the wavelength of pristine and R6G-sensitized MoS_2 photodetectors. The inset of panel b shows the UV−vis absorption spectra of the R6G film coated onto glass.

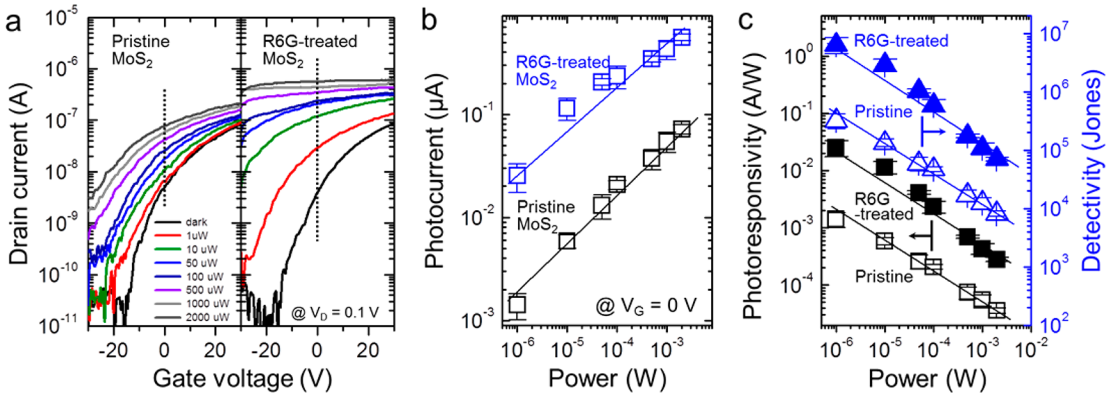

Figure 3. (a) Photoinduced transfer characteristics of the pristine and R6G-sensitized MoS_2 photodetectors under different illumination source optical powers ($\lambda = 520$ nm). (b) Photocurrent at $V_G = 0$ V and (c) photoresponsivity and photodetectivity as a function of the optical power for the pristine and R6G-sensitized MoS_2 photodetectors.

zero gate voltage in the transfer curves. As with the wavelength dependence, the photoresponse of the device increased dramatically after the deposition of the R6G organic dyes because the photoinduced carriers generated in the R6G dye molecules were transferred to the MoS_2 channel. The linear relationship between I_{ph} and P_{light} confirmed that the photocurrent was determined by the quantity of photogenerated carriers created under illumination. The photocurrent obtained from the R6G-sensitized MoS_2 photodetector was more than an order of magnitude higher than the photocurrent obtained from the pristine MoS_2 photodetector (Figure 3b). Figure 3c shows the calculated photoresponsivity and photodetectivity of the pristine and R6G-sensitized MoS_2 photodetectors, which exhibited an enhanced photoresponsivity and photodetectivity

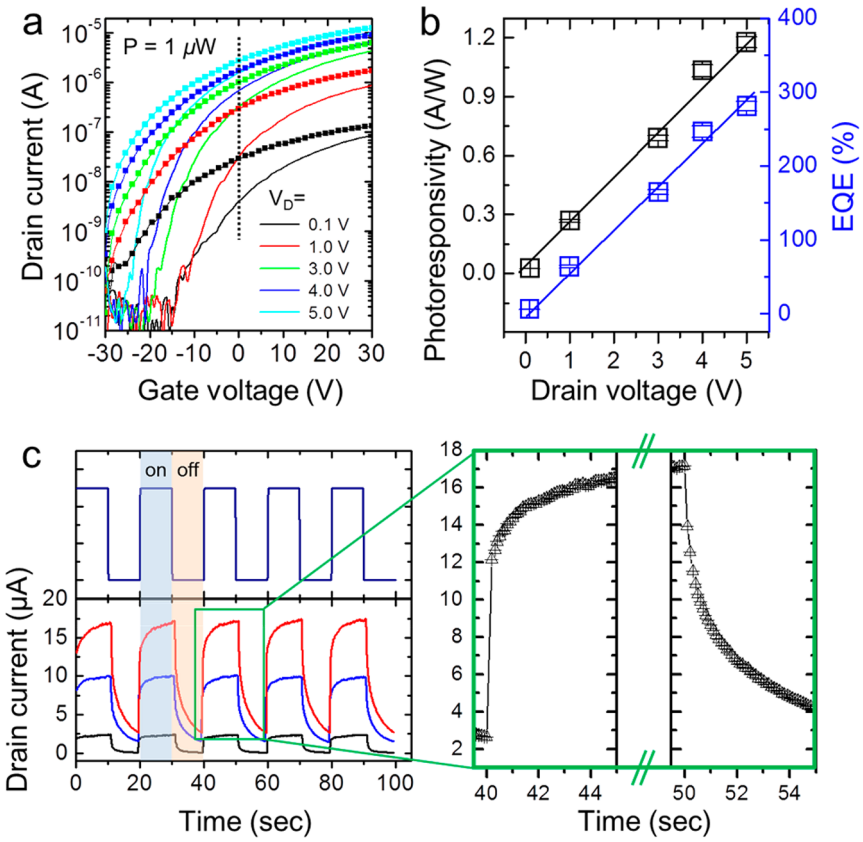

Figure 4. (a) Photoinduced transfer characteristics of the R6G-sensitized MoS_2 photodetectors at different drain voltages under illumination at λ = 520 nm and P = 1 μW. The curves with (without) dots indicate the total (dark) currents of the devices. (b) Photoresponsivity and EQE at V_G = 0 V as a function of the applied drain voltage. (c) Photoswitching characteristics of the R6G-sensitized MoS_2 photodetectors at three different drain voltages (black = 1 V, blue = 3 V, and red = 5 V) under alternating dark and light illumination (λ = 520 nm and P = 1 mW).

in the R6G-sensitized MoS_2 photodetector after the deposition of the R6G organic dye. For example, the photoresponsivity and photodetectivity of the R6G-sensitized MoS_2 detector were 2.5 $\times$ 10^{-2} A W^{-1} and 6.4 $\times$ 10^6 Jones at an optical power of 1 μW, respectively.

The photosensitivity of the R6G-sensitized MoS_2 photodetector increased upon application of a drain voltage exceeding 0.1 V. The photoinduced transfer curves of the R6G-sensitized MoS_2 under dark and 520 nm illumination (P = 1 μW) were obtained under a range of drain voltages between 0.1 and 5 V, as shown in Figure 4a. The photocurrent measured at V_G = 0 V was used to calculate the photoresponsivity, photodetectivity, and EQE. The photoresponsivity increased linearly with V_D up to 5 V, although the V_D values exceeding 5 V induced device breakdown (Figure 4b). Larger V_D values provided a stronger driving force for the transfer of photogenerated electrons to the electrode or a stronger suppression of photogenerated electron recombination. We achieved a photoresponsivity of 1.17 A W^{-1} and a photodetectivity of 1.5 $\times$ 10^7 Jones at V_D = 5 V. Importantly, a very high quantum efficiency of 280% at V_D = 5 V was obtained in the hybrid device. This value was 50 times higher than that measured at V_D = 0.1 V (Figure 4b). Note that we measured the total EQE (effective quantum efficiency), which differs from the known external quantum efficiency and is defined as the product of the external quantum efficiency and the gain of the device. In this paper, we calculated the EQE from the measured total photocurrent, *i.e.*, EQE (%) = $(I_{ph}/e)/(P_{light}/h\upsilon)$ $\times$ 100. A comparison with the quantum efficiency of the pristine MoS_2 photodetector revealed that the device gain exceeded a few hundreds. The measured performances could be further improved by using pristine MoS_2 with good electrical properties.

Finally, the time-resolved photoresponse of the R6G-sensitized MoS_2-based photodetector was investigated over multiple illumination cycles at different V_D values, as shown in Figure 4c. The current rose to a high value (ON state) under illumination and then returned to a low value as the light was turned off (OFF state). The generated photocurrent increased with V_D. For example, the photocurrent increased from 2.4 to 17.2 μA as V_D increased from 1 to 5 V. The response was characterized by a typical rise time of 5.1 μs and a fall time of 2.3 s for V_D = 5 V. The rising and falling regions of the curve could be fitted to a single exponential function. For comparison, the temporal response of the

pristine MoS_2 device was measured as shown in Supporting Information Figure S6. No obvious changes in the rise and fall times were observed, even though the overall photocurrent of the hybrid photodetector increased by a factor of 6 compared with that of the pristine device. The relatively slow fall time of the MoS_2-based photodetector was attributed to the slow recombination process of the photoexcited electrons in MoS_2 (or the high gain mechanism). The slow fall time could be improved by applying a short gate pulse, as reported in ref 5. Moreover, the ON−OFF switching behavior was retained over multiple cycles, indicating the robustness and reproducibility of the photodetector performance. R6G undergoes photodegradation under light illumination, which may decrease the performance of the R6G-treated MoS_2 photodetector.[35,36] Therefore, encapsulation and isolation of the hybrid photodetectors from ambient oxygen is necessary to ensure good photostabilities.[37]

CONCLUSIONS

In conclusion, we demonstrated the preparation of a novel organic R6G-sensitized MoS_2 photodetector. The application of R6G dyes to the MoS_2 surfaces dramatically enhanced the photoresponse of the pristine MoS_2 photodetector *via* photoinduced charge transfer from R6G to MoS_2. The optimized device showed a maximum responsivity of 1.17 AW^{-1}, a photodetectivity of 1.5×10^7 Jones, an EQE of 280% at a wavelength of 520 nm, and a photoresponse across a broad spectral range from 980 to 405 nm. The method described here presents a significant step forward toward the achievement of next-generation high-performance photodetectors based on 2D nanomaterials.

EXPERIMENTAL SECTION

Fabrication of MoS_2 Photodetector. Single-layer MoS_2 nanosheets were mechanically exfoliated from bulk MoS_2 crystals (natural single crystals, SPI Supplies) and mounted on highly p-doped silicon substrates bearing a 300 nm thick SiO_2 layer. Monolayer MoS_2 nanosheets were identified by optical microscopy (Eclipse LV199, Nikon). The source (S) and drain (D) Cr/Au metal electrodes (5/50 nm thick) were fabricated using e-beam lithography and lift-off. A photoresist layer (PMMA A5 495, MicroChem) was initially coated by spin-coating. The substrates were then baked at 180 °C for 3 min. Patterning was performed using e-beam lithography (JSM-6390, JEOL/NPGS, JC Nabity) with a 30 kV beam, and the substrates were exposed to ultraviolet (UV) light and developed in an IPA/MIBK = 1:3 solution for 40 s. After developing the patterns, the S/D electrodes were deposited using a thermal evaporator. The lift-off process was performed with acetone. Finally, the devices were annealed under 60 sccm Ar and 6 sccm H_2 flows at 300 °C for 2 h. The channel length (L) and width (W) were 6.25 and 13 μm, respectively. A 1 mM solution of rhodamine 6G (R6G) (99%, Sigma-Aldrich) was prepared by dissolving R6G in DI water. The R6G solution was drop-cast onto the single-layer MoS_2 device on a hot plate at 70 °C.

Characterization. The quality and thicknesses of the MoS_2 nanosheets were investigated using atomic force microscopy (Innova, Veeco) and Raman spectroscopy (RM 1000-Invia, Renishaw). A 532 nm excitation laser was used to conduct the Raman spectroscopy measurements. All current−voltage (I−V) and photodetection properties of the MoS_2 photodetectors were measured using Keithley 2400 and 246 source/measure units under dark and illuminated conditions. The light sources were set up using dot lasers having wavelengths between 405 and 980 nm and operated at an optical power of 2 mW. The optical power was controlled between 1 μW and 2 mW using an optical ND filter (NDC-100C-4M, Thorlabs).

Conflict of Interest: The authors declare no competing financial interest.

Supporting Information Available: Calculation of the DOS and figures. This material is available free of charge *via* the Internet at http://pubs.acs.org.

Acknowledgment. This work was supported by the Center for Advanced Soft-Electronics funded by the Ministry of Science, ICT and Future Planning as Global Frontier Project (2013M3A6A5073177 and 2011-0031630), Global Frontier Program through the Global Frontier Hybrid Interface Materials (GFHIM) (2013M3A6B1078873) of the National Research Foundation of Korea (NRF) funded by the MOSIP, and Basic Science Research Program (2009-0083540) of the National Research Foundation of Korea (NRF) funded by the Ministry of Education, Science, and Technology, Korea.

REFERENCES AND NOTES

1. Wu, P.; Dai, Y.; Ye, Y.; Yin, Y.; Dai, L. Fast-Speed and High-Gain Photodetectors of Individual Single Crystalline Zn_3p_2 Nanowires. *J. Mater. Chem.* **2011**, *21*, 2563–2567.
2. Zhang, W.; Chuu, C. P.; Huang, J. K.; Chen, C. H.; Tsai, M. L.; Chang, Y. H.; Liang, C. T.; Chen, Y. Z.; Chueh, Y. L.; He, J. H. Ultrahigh-Gain Photodetectors Based on Atomically Thin Graphene-MoS_2 Heterostructures. *Sci. Rep.* **2014**, *4*, 3826–3833.
3. Xia, F.; Mueller, T.; Lin, Y. M.; Valdes Garcia, A.; Avouris, P. Ultrafast Graphene Photodetector. *Nat. Nanotechnol.* **2009**, *4*, 839–843.
4. Hu, P.; Wang, L.; Yoon, M.; Zhang, J.; Feng, W.; Wang, X.; Wen, Z.; Idrobo, J. C.; Miyamoto, Y.; Geohegan, D. B. Highly Responsive Ultrathin Gas Nanosheet Photodetectors on Rigid and Flexible Substrates. *Nano Lett.* **2013**, *13*, 1649–1654.
5. Lopez-Sanchez, O.; Lembke, D.; Kayci, M.; Radenovic, A.; Kis, A. Ultrasensitive Photodetectors Based on Monolayer MoS_2. *Nat. Nanotechnol.* **2013**, *8*, 497–501.
6. Radisavljevic, B.; Radenovic, A.; Brivio, J.; Giacometti, V.; Kis, A. Single-Layer MoS_2 Transistors. *Nat. Nanotechnol.* **2011**, *6*, 147–150.
7. Chhowalla, M.; Shin, H. S.; Eda, G.; Li, L. J.; Loh, K. P.; Zhang, H. The Chemistry of Two-Dimensional Layered Transition Metal Dichalcogenide Nanosheets. *Nat. Chem.* **2013**, *5*, 263–275.
8. Laocharoensuk, R.; Palaniappan, K.; Smith, N. A.; Dickerson, R. M.; Werder, D. J.; Baldwin, J. K.; Hollingsworth, J. A. Flow-Based Solution-Liquid-Solid Nanowire Synthesis. *Nat. Nanotechnol.* **2013**, *8*, 660–666.
9. Omachi, H.; Nakayama, T.; Takahashi, E.; Segawa, Y.; Itami, K. Initiation of Carbon Nanotube Growth by Well-Defined Carbon Nanorings. *Nat. Chem.* **2013**, *5*, 572–576.
10. Lee, G. H.; Yu, Y. J.; Cui, X.; Petrone, N.; Lee, C. H.; Choi, M. S.; Lee, D. Y.; Lee, C.; Yoo, W. J.; Watanabe, K. Flexible and Transparent MoS_2 Field-Effect Transistors on Hexagonal Boron Nitride-Graphene Heterostructures. *ACS Nano* **2013**, *7*, 7931–7936.
11. George, P. A.; Strait, J.; Dawlaty, J.; Shivaraman, S.; Chandrashekhar, M.; Rana, F.; Spencer, M. G. Ultrafast Optical-Pump Terahertz-Probe Spectroscopy of the Carrier Relaxation and Recombination Dynamics in Epitaxial Graphene. *Nano Lett.* **2008**, *8*, 4248–4251.

12. Bonaccorso, F.; Sun, Z.; Hasan, T.; Ferrari, A. Graphene Photonics and Optoelectronics. *Nat. Photonics* **2010**, *4*, 611–622.
13. Mueller, T.; Xia, F.; Avouris, P. Graphene Photodetectors for High-Speed Optical Communications. *Nat. Photonics* **2010**, *4*, 297–301.
14. Xia, F.; Mueller, T.; Golizadeh-Mojarad, R.; Freitag, M.; Lin, Y.-m.; Tsang, J.; Perebeinos, V.; Avouris, P. Photocurrent Imaging and Efficient Photon Detection in a Graphene Transistor. *Nano Lett.* **2009**, *9*, 1039–1044.
15. Nair, R. R.; Blake, P.; Grigorenko, A. N.; Novoselov, K. S.; Booth, T. J.; Stauber, T.; Peres, N. M. R.; Geim, A. K. Fine Structure Constant Defines Visual Transparency of Graphene. *Science* **2008**, *320*, 1308.
16. Echtermeyer, T.; Britnell, L.; Jasnos, P.; Lombardo, A.; Gorbachev, R.; Grigorenko, A.; Geim, A.; Ferrari, A.; Novoselov, K. Strong Plasmonic Enhancement of Photovoltage in Graphene. *Nat. Commun.* **2011**, *2*, 458–462.
17. Liu, Y.; Cheng, R.; Liao, L.; Zhou, H.; Bai, J.; Liu, G.; Liu, L.; Huang, Y.; Duan, X. Plasmon Resonance Enhanced Multicolour Photodetection by Graphene. *Nat. Commun.* **2011**, *2*, 579–585.
18. Furchi, M.; Urich, A.; Pospischil, A.; Lilley, G.; Unterrainer, K.; Detz, H.; Klang, P.; Andrews, A. M.; Schrenk, W.; Strasser, G. Microcavity-Integrated Graphene Photodetector. *Nano Lett.* **2012**, *12*, 2773–2777.
19. Yin, Z.; Li, H.; Li, H.; Jiang, L.; Shi, Y.; Sun, Y.; Lu, G.; Zhang, Q.; Chen, X.; Zhang, H. Single-Layer MoS_2 Phototransistors. *ACS Nano* **2012**, *6*, 74–80.
20. Hu, P.; Wen, Z.; Wang, L.; Tan, P.; Xiao, K. Synthesis of Few-Layer Gase Nanosheets for High Performance Photodetectors. *ACS Nano* **2012**, *6*, 5988–5994.
21. Jariwala, D.; Sangwan, V. K.; Lauhon, L. J.; Marks, T. J.; Hersam, M. C. Emerging Device Applications for Semiconducting Two-Dimensional Transition Metal Dichalcogenides. *ACS Nano* **2014**, *8*, 1102–1120.
22. Konstantatos, G.; Badioli, M.; Gaudreau, L.; Osmond, J.; Bernechea, M.; de Arquer, F. P. G.; Gatti, F.; Koppens, F. H. Hybrid Graphene-Quantum Dot Phototransistors with Ultrahigh Gain. *Nat. Nanotechnol.* **2012**, *7*, 363–368.
23. Zheng, K.; Meng, F.; Jiang, L.; Yan, Q.; Hng, H. H.; Chen, X. Visible Photoresponse of Single-Layer Graphene Decorated with TiO_2 Nanoparticles. *Small* **2013**, *9*, 2076–2080.
24. Fang, Z.; Liu, Z.; Wang, Y.; Ajayan, P. M.; Nordlander, P.; Halas, N. J. Graphene-Antenna Sandwich Photodetector. *Nano Lett.* **2012**, *12*, 3808–3813.
25. Prins, F.; Buscema, M.; Seldenthuis, J. S.; Etaki, S.; Buchs, G.; Barkelid, M.; Zwiller, V.; Gao, Y.; Houtepen, A. J.; Siebbeles, L. D. A.; van der Zant, H. S. J. Fast and Efficient Photodetection in Nanoscale Quantum-Dot Junctions. *Nano Lett.* **2012**, *12*, 5740–5743.
26. Nguyen, W. H.; Bailie, C. D.; Burschka, J.; Moehl, T.; Grätzel, M.; McGehee, M. D.; Sellinger, A. Molecular Engineering of Organic Dyes for Improved Recombination Lifetime in Solid-State Dye-Sensitized Solar Cells. *Chem. Mater.* **2013**, *25*, 1519–1525.
27. Yu, J.; Zhang, X.; Hao, X.; Zhang, X.; Zhou, M.; Lee, C.-S.; Chen, X. Near-Infrared Fluorescence Imaging Using Organic Dye Nanoparticles. *Biomaterials* **2014**, *35*, 3356–3364.
28. Chua, S.-L.; Zhen, B.; Lee, J.; Bravo-Abad, J.; Shapira, O.; Soljačić, M. Modeling of Threshold and Dynamics Behavior of Organic Nanostructured Lasers. *J. Mater. Chem. C* **2014**, *2*, 1463–1473.
29. Liu, X.; Zhang, W.; Uchida, S.; Cai, L.; Liu, B.; Ramakrishna, S. An Efficient Organic-Dye-Sensitized Solar Cell with *in Situ* Polymerized Poly(3,4-ethylenedioxythiophene) as a Hole-Transporting Material. *Adv. Mater.* **2010**, *22*, E150–E155.
30. Lee, H. S.; Min, S.-W.; Chang, Y.-G.; Park, M. K.; Nam, T.; Kim, H.; Kim, J. H.; Ryu, S.; Im, S. MoS_2 Nanosheet Phototransistors with Thickness-Modulated Optical Energy Gap. *Nano Lett.* **2012**, *12*, 3695–3700.
31. Zhang, W.; Huang, J. K.; Chen, C. H.; Chang, Y. H.; Cheng, Y. J.; Li, L. J. High-Gain Phototransistors Based on a CVD MoS_2 Monolayer. *Adv. Mater.* **2013**, *25*, 3456–3461.
32. Perdew, J. P.; Burke, K.; Ernzerhof, M. Generalized Gradient Approximation Made Simple. *Phys. Rev. Lett.* **1996**, *77*, 3865–3868.
33. Grimme, S. Density Functional Theory with London Dispersion Corrections. *Wiley Interdiscip. Rev.: Comput. Mol. Sci.* **2011**, *1*, 211–228.
34. Konstantatos, G.; Sargent, E. H. Nanostructured Materials for Photon Detection. *Nat. Nanotechnol.* **2010**, *5*, 391–400.
35. Avnir, D.; Levy, D.; Reisfeld, R. The Nature of the Silica Cage As Reflected by Spectral Changes and Enhanced Photostability of Trapped Rhodamine 6G. *J. Phys. Chem.* **1984**, *8*, 5956–5959.
36. Li, Y.; Li, Y. L.; Araujo, C. M.; Luo, W.; Ahuja, R. Single-Layer MoS_2 as an Efficient Photocatalyst. *Catal. Sci. Technol.* **2013**, *3*, 2214–2220.
37. Zhao, Y.; Xie, Y.; Bao, Z.; Tsang, Y. H.; Tsang, Y. H.; Xie, L.; Chai, Y. Enhanced SERS Stability of R6G Molecules with Monolayer Graphene. *J. Phys. Chem. C* **2014**, *118*, 11827–11832.